ADVANCED QUANTUM TECHNOLOGIES
www.advquantumtech.com

Controllable Delay and Polarization Routing of Single Photons

Julian Maisch, Hüseyin Vural, Michael Jetter, Peter Michler, Ilja Gerhardt, and Simone Luca Portalupi*

Full control of single photons is important in quantum information and quantum networking. In particular, controlling the photon–atom interaction can be an appealing means to realize more complex quantum experiments. As a matter of example, the storage of photons into atomic media represents one key approach to memory-assisted quantum communication and computing. Here it is shown that the propagation of single photons from a semiconductor quantum dot can be deliberately controlled by an atomic vapor under the application of an external magnetic field. The present results enable the use of an atomic vapor as a precise and reliable wavelength selective delay and allows for routing the single photons according to their polarization and the external magnetic field. With an overall delay of 25 ns, it is possible to fine-tune the arrival time of the photons by more than 600 ps which matches the scale of the quantum dot's lifetime. The experimental data are fully reproduced by a theoretical model.

1. Introduction

Single photons are an essential ingredient in quantum information processing. Indeed, encoding information into single photons will result in highly secure data transfer which becomes particularly appealing for the implementation of quantum cryptography and communication schemes.[1] A strong improvement in up-scaling the experimental complexity needs the generation of photons in a deterministic or turnstile way, such that a single photon can be generated on-demand. This forms the key advantage of single emitter based single photon sources against so-called parametric down-conversion sources. Typically on-demand single photon sources originate from single atoms[2] and ions, over molecules[3] to defect centers[4] and quantum dots.[5] Since quantum dots (QDs) are based on semiconductor technology, they hold the promise to be integrated onto chip-scale devices. Furthermore, their potential to generate polarization entangled photons[6,7] opens the route for a variety of quantum information schemes, which are enabled by this quantum phenomenon.

Current state-of-the-art QDs exhibit high brightness, high indistinguishability,[8–10] and entanglement fidelity.[11] Quantum dots therefore represent a very appealing source of non-classical light. On the other hand, in many quantum applications, such as quantum repeaters, the implementation of a deterministic quantum memory is beneficial. At present, the relatively short coherence times of the QD's spin may limit their performance as storage media. In contrast, atomic systems with their high coherence and long storage times could provide this option.[12] Still, the implementation of a full storage experiment is a challenging task. For instance, the intensity mismatch between single photons and the required high power control fields complicate the experimental realization. Another limiting factor is the bandwidth mismatch, when, for example, broad photons have to be stored in a spectrally narrow medium. Before the realization of an efficient quantum memory, it is therefore of fundamental importance to fully understand the physics behind the atom–photon interaction. For example, it has been shown that photon propagation near atomic transitions can result in an observable photonic delay. First results with laser pulses[13–16] have set the basis for more recent experiments where single photons were slowed down within alkali vapors.[17–21] These experiments showed the potential of implementing a hybrid quantum system combining single photons from quantum dots with their atomic counterparts.

Here we report on the experimental implementation of a fine-tunable delay with simultaneous photonic routing in a hot atomic cesium vapor. While the control of the vapor temperature allows for reaching high values of photonic delay[21] the simultaneous use of a magnetic field results in a faster and more reliable knob for controlling the photon arrival time. Controlling precisely this

J. Maisch, H. Vural, Dr. M. Jetter, Prof. P. Michler, Dr. S. L. Portalupi
Institut für Halbleiteroptik und Funktionelle Grenzflächen (IHFG)
Center for Integrated Quantum Science and Technology (IQST) and SCoPE
University of Stuttgart
Allmandring 3, D-70569 Stuttgart, Germany
E-mail: j.maisch@ihfg.uni-stuttgart.de
Dr. I. Gerhardt
3rd Institute of Physics
Center for Integrated Quantum Science and Technology (IQST)
University of Stuttgart
Pfaffenwaldring 57, D-70569 Stuttgart, Germany

The ORCID identification number(s) for the author(s) of this article can be found under https://doi.org/10.1002/qute.201900057

DOI: 10.1002/qute.201900057

property is of relevance when performing two-photon interference, that is, the basic building block of quantum operations, where the arrival time of the photons on the beamsplitter needs to be precisely synchronized.

Furthermore, the polarization-dependent control on the single-photon propagation direction constitutes a proof-of-principle demonstration which can have applications in photonic routing, or photon multiplexing.[22] The experiments are conducted with a semiconductor quantum dot as an on-demand source of single photons. The delay and the routing is implemented by a 250 mm long Cs-vapor cell in a externally controllable magnetic field. Depending on the external magnetic field, the two polarization components of the light are affected differently. This feature can be deliberately controlled and fine-adjusted by the external magnetic field. All results are supported by a theoretical model which additionally foresees the potentials of improving the fine-tuning capabilities.

2. Theory

The refractive index in a hot atomic vapor is tied to the strong absorption lines and the dispersion in the medium. This well-known phenomenon is usually represented by a division into a real and an imaginary part of the refractive index—the Kramers–Kronig relation. The index can be divided as $n = n' + in''$. With the electric susceptibility, χ, this is approximately equivalent to $n = 1 + 2\pi\chi$, where χ is represented as

$$\chi = \frac{Ne^2/2m\omega_0}{(\omega_0 - \omega) - i\gamma}. \tag{1}$$

Here, N represents the number of involved atoms, e is the electron charge, ω_0 represents the transition, and ω the laser frequency. γ represents the radiative lifetime of the excited state. Therefore, in other words, the refractive index is represented by the two components

$$n' = 1 + \frac{\pi N e^2}{2m\omega_0\gamma}\frac{2(\omega_0 - \omega)\gamma}{(\omega_o - \omega)^2 + \gamma^2} \tag{2}$$

$$n'' = \frac{\pi N e^2}{2m\omega_0\gamma}\frac{\gamma^2}{(\omega_0 - \omega)^2 + \gamma^2}. \tag{3}$$

The group velocity inside a medium of group index $n_g = n' + \omega dn'/d\omega$ is known to be given as $c_g = c/n_g$. When the group index is larger than unity "slow light" can be observed,[17,18,21] while for an index below unity "fast light" is expected.[23,24]

Under the influence of a longitudinal magnetic field, the Zeeman effect leads to a spectral splitting of the atomic lines. This naturally influences not only the absorption but also the dispersive components of the refractive index. Both of the two split dispersion components act differently on circularly polarized light. This holds consequently also for linearly polarized light, which can be represented as a linear-combination of two circular fields. In summary, this leads to an effective rotation of light which is based on the Faraday effect.[25] This has been used in Faraday filters and the symmetry breaking allows to utilize this effect for optical isolation on or close to the atomic resonance.[26]

Both schemes analyze the input of linearly polarized light and rely on the effective rotation of the linear component by the atomic medium. A linear analyzer behind a vapor cell, which is orthogonally oriented to the input polarization to the vapor cell, can be passed and the net rotation is quantified. Similarly, the effect allows for laser locking by the individual analysis of the circular polarization components of the beam. This is known as a dichroic atomic vapor laser lock (DAVLL, ref. [27,28]). Here, the circular components are analyzed behind the cell by the combination of a quarter-waveplate and a polarizing beamsplitter. Each of the two circular components shows a different spectral shift and the difference of both signals forms dispersive lines for each transition. The zero crossing is usually a reliable lock-point and is used for laser locking.[29]

Naturally, also the group velocity of the light is affected by the dispersion in the atomic medium. In the case of a monochromatic input field, it can be determined by calculating the effective refractive indexes of the different atomic transitions and they can be used to calculate the group velocity. Under broadband, that is, non-monochromatic, illumination different spectral components are affected differently. The resulting delay is represented by an integration of the individual delays over the entire spectrum and is generally more complex than in the monochromatic case.[30] When this is mathematically estimated it becomes clear that a) the longer the delay, the longer a light pulse is delayed and the more it smears out, b) these characteristic fingerprints can be observed and the pulse shape is affected in a non-trivial way.[21]

The above description of slow light is not limited on a single frequency light input. In addition, when a magnetic field is applied to the hot atomic vapor, both circular components (even when the light fields are of the same frequency) are influenced differently. Therefore, in the following both polarization components are analyzed.

The analysis is accompanied with theoretical calculations of the delay. Aim of the simulation is to obtain the respective shapes after propagation through the atomic medium. The calculations assume a random-walk model of the spectral position of the quantum dot.[21] Due to fluctuations of the electric and magnetic field in the environment of a QD its energy levels shift randomly—an effect which is often described as spectral diffusion. Therefore, the carrier frequency of photons changes over time between different emission events. This results in a Gaussian frequency spectrum whereas in the Fourier limit a Lorentzian shape is expected. In the simulation model each single photon is assumed to be Fourier limited. That implies an exponential decaying temporal form and a Lorentzian frequency spectrum. The integral of all single shapes with a respective statistical weight results in the profile of the photon ensemble. The implementation of the conducted simulations follows this picture. The starting point for the propagation of one single photon is the basic Fourier pair of an exponential decay in time domain linked with a Lorentzian shape in frequency domain.The vapor is regarded as linear medium which allows a full description of the propagation via the complex refractive index. In this case the software tool ElecSus[33] was utilized to provide the values of real and imaginary part ($n(\nu)$ and $\alpha(\nu)$). With that it is possible to calculate the spectrum after propagation through the vapor of length L

$$\chi_{\text{in}}(\omega) \rightarrow \chi_{\text{out}}(\omega) = \chi_{\text{in}}(\omega) \cdot e^{in_c kL} \tag{4}$$

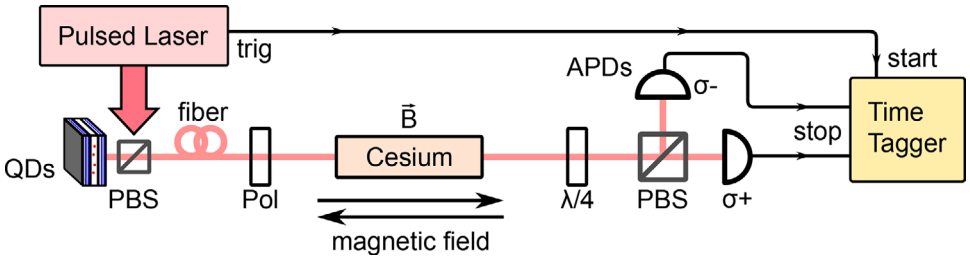

Figure 1. Experimental setup for time-correlated single photon counting (TCSPC). The quantum dot (QD) is resonantly excited. Through the polarizer (Pol) the single photons enter the cesium vapor cell linearly polarized. A variable magnetic field can be applied parallel or anti-parallel to the propagation direction. Behind the vapor cell the quarter wave plate ($\lambda/4$) projects the circular polarizations onto orthogonal linear components. These are separated onto the two APDs via the polarizing beamsplitter (PBS). The signals are recorded by time-tagging.

$$\text{with} \qquad n_c = n(\omega) + \frac{i}{2k}\alpha(\omega). \tag{5}$$

Then, an inverse Fourier transformation provides the temporal form of the propagated photons. This procedure is repeatedly performed for an ensemble of photons where each one is assumed to be Fourier limited with a certain carrier frequency. This carrier frequency is drawn from a random Gaussian distribution which can be chosen according to the measurement result of the emission spectrum.

3. Experiment

The experimental configuration is shown in **Figure 1**. The input light was linearly polarized and the light was analyzed in its circular components with the aid of a quarter wave plate and a polarizing beamsplitter. For the initial alignment a laser and commercial photo diodes with variable gain were used, while the atomic cell was at a low temperature, or the laser was several tens of GHz spectrally detuned from the atomic resonance. The light was supplied to the experiment with a single mode fiber.

The atomic vapor cell for these experiments was made of borosilicate glass and has a length of 250 mm. The cell was heated by four round copper blocks which were approximately equally spaced along the length of the cell. The two most outer copper blocks heated the cell windows and prevented condensation of the atomic cesium on them. The coldest spot of the cell was aligned with the filling stem of the cell by a piece of aluminum foil which touched the colder parts of the coil from the inside.

When the atomic vapor was heated, an atomic transmission spectrum with Doppler broadened lines was observed. The cesium D_1-line shows the well-characterized ground state splitting of 9.192 GHz, plus the excited state splitting of 1.2 GHz. Since the latter is larger than the Doppler broadening of the vapor—at least under ambient conditions—usually four lines are observed. At higher temperatures, the excited state transitions merged and only two dominant absorption features were observed. Between them, the transmission window showed the typical $1/\delta\nu^2$ detuning frequency dependence and a small window was kept open, which was used to perform the experiments below. This was also the window where slow light could be efficiently observed, since there the effective group index $dn/d\omega$ was approximately twice as large as besides the atomic transitions.[31]

It was possible to apply a magnetic field to the cell, such that the Zeeman components were split. This was realized with a long solenoid of enameled copper wire (0.8 mm ∅). The solenoid was thermally isolated with Teflon supports from the cell heater. After some hours of heating a stable temperature was reached. It is worth mentioning that the current through the coil also heated the system, which in turn affected the temperature during the application of a magnetic field. This fact became relevant when the magnetic field was changed.

The single photon source used here was a strain-tunable In(Ga)As/GaAs quantum dot which was grown by metal-organic vapor-phase epitaxy.[32] The light-extraction was facilitated by two distributed Bragg reflector (DBR) layers: the quantum dot layer was in the middle of a GaAs λ-cavity surrounded by the DBRs (20 pairs bottom, 4 pairs top). The quantum dot distribution ranged from 885 to 910 nm, making it possible to find dots emitting in the vicinity of the Cs-D_1 transitions. To allow the precise matching of the atomic lines, the sample was thinned mechanically and glued on a piezo actuator, providing wavelength tuning via strain. A pulsed laser with a repetition rate of approximately 13 MHz (by pulse picking a standard 80 MHz Ti:Sapphire laser) excited the quantum dot resonantly at the π-pulse, while a weak, non-resonant second laser stabilized the transition. Simultaneously, it prepared a charged exciton transition by exciting charge carriers which initially charged the QD. For single-photon detection two standard single photon counting modules were utilized (Excelitas SPCM-AQRH), in combination with time-tagging electronics (Swabian Instruments "Time Tagger 20") to evaluate the photon statistics.

First, the vapor was investigated spectroscopically with an applied magnetic field. **Figure 2**a shows the setup where the light enters the vapor horizontally polarized. The light polarization was altered due to the Faraday effect and was detected by a pair of photodiodes behind a polarizing beamsplitter. The resulting polarization-dependent transmission was exemplarily shown for $T = 80\,°\text{C}$ and $B = 8$ mT in Figure 2b. The spectra of both components show oscillating modulations besides the well-known absorption profile. The transmission oscillated between zero and the maximal transmission, dictated by the overall vapor absorption. The observed frequency-dependent polarization rotation was a consequence of a phase difference between the circular polarization components of the light, due to the circular birefringence induced by the magnetic field. The same effect caused a polarization-dependent delay in measurements with pulsed light as observed with laser light on ref. [14,15].

Then, the experiment was performed with single photons. **Figure 3**a shows the measured pulsed second-order

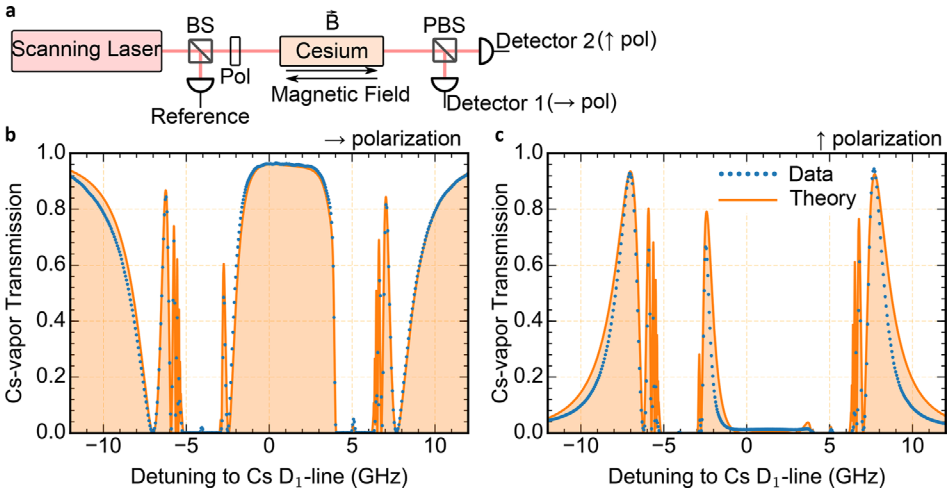

Figure 2. a) Setup for measuring the Cs-D_1 absorption spectra of the polarization components. The polarizer (Pol) ensures that the light enters the vapor cell linearly polarized. The polarizing beamsplitter (PBS) separates the orthogonal polarization components at the two detectors. b) and c) Measured (dotted lines) and calculated (solid lines) spectra for the Cs-D_1 absorption in a 250 mm long vapor cell at temperature of 80 °C and a longitudinal magnetic field of 8 mT. The two panels show the separated polarization components: b) horizontal and c) vertical.

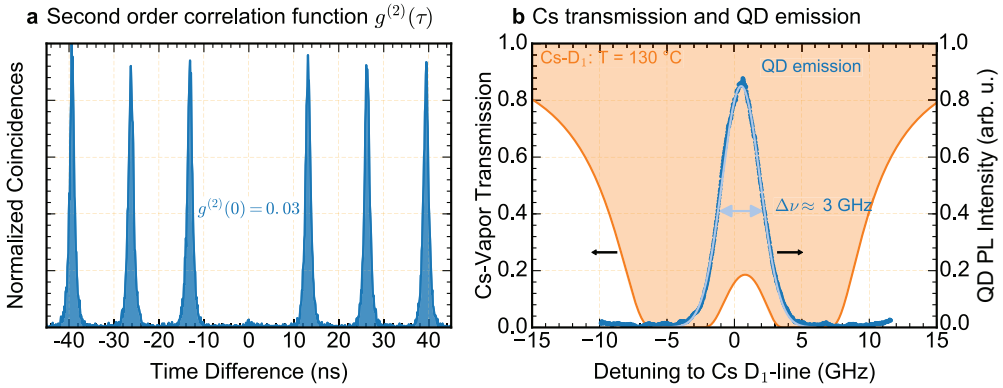

Figure 3. a) Intensity auto-correlation of the single photons. b) High resolution resonance fluorescence spectrum of the QD under investigation (blue) and the Gaussian fit (light blue, solid line). For comparison, the calculated absorption spectrum of the Cs-D_1 line is shown in the background (orange).

correlation function of the emission. The vanishing central peak ($g^{(2)}(0) = 0.03 \pm 0.01$) clearly proves the single-photon nature of the emission. The evaluation of the $g^{(2)}$-histogram was done by integrating the coincidences within each laser repetition, that is, determining the peak areas. Figure 3b shows the spectrum of the QD. The solid line represents a Gaussian fit to the data. A nearly Gaussian profile with 3 GHz width was observed: these were the data utilized in the theoretical modeling. This well-known shape can be attributed to the presence of spectral diffusion. As comparison, the Cs absorption at 130 °C is depicted, the temperature at which the cell was kept during the single-photon experiments. The width of the QD emission was on the same scale as the width of the transmission window.

Due to dispersion in the vapor, the group velocity of photons inside the medium was reduced. Therefore, slow light was observed. In the absence of a magnetic field, the delay through the heated atomic vapor amounted to ≈ 25 ns. It was noteworthy that this delay was similarly observed in a previous work [21].

When a magnetic field was applied, it influenced the two circular components of the propagating light differently. This resulted in different refractive indices and consequently in different group velocities for both components. This opened the possibility to fine-tune the delay. In the given TCSPC setup (Figure 1) a fine-tuning range at the scale of the QD's lifetime $\tau \approx 500$ ps was aimed at. The polarizer before the vapor cell ensured that the photons entered horizontally polarized. Afterward a $\lambda/4$-plate and a polarizing beamsplitter projected the both circular components ($\sigma+$ and σ-) onto two separate APDs. The recorded signals of slow light under different magnetic fields are shown in **Figure 4**a–c. While both signals overlapped for zero magnetic field (b), the altered delay if a magnetic field of B= +16 mT was applied was clearly observed (a). Reversing the orientation of the magnetic field (i.e., $B = -16$ mT was applied (c)), simultaneously inversed the delay of the two polarization components. Due to the complex absorption spectrum, the lines were differently affected. For the maximal magnetic field a gap of ≈ 600 ps between both components was reached. This matched the targeted order of magnitude of the QD's lifetime. However, the two wave packets were not entirely separated. This was due to the vapor dispersion which caused distortions of the photons resulting in an elongated decay.

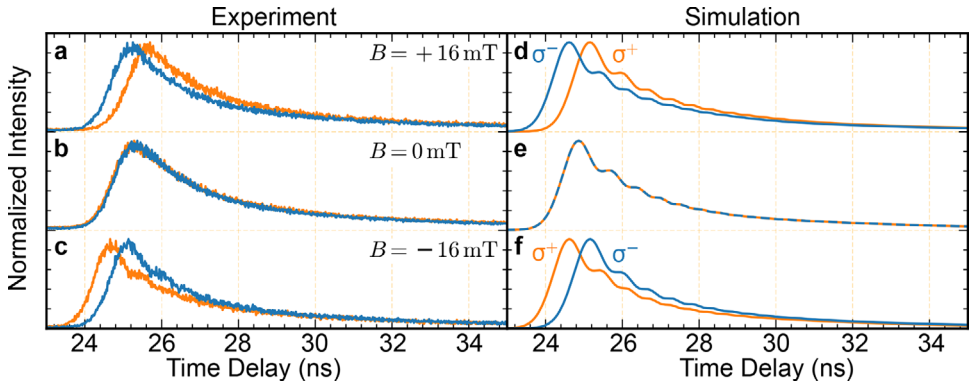

Figure 4. TCSPC measurements with the setup in Figure 1. Three configurations of the magnetic field: a) parallel to the direction of propagation, b) without magnetic field, and c) anti-parallel. d–f) show the corresponding simulation results.

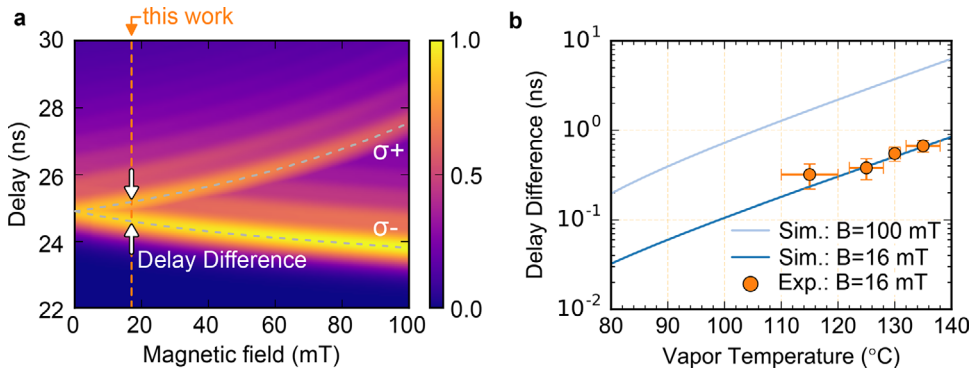

Figure 5. a) Simulated delay of photons with σ^+- and σ^--polarization versus the applied magnetic field. The temperature $T = 130$ °C corresponds with the experimental conditions in Figure 4. The dashed line indicates the operating point in the presented experiment. b) Delay difference between σ^+- and σ^--components over the vapor temperature. Circles (orange) indicate experiments (as in Figure 4) at various temperatures for an applied magnetic field of 16 mT. The blue (light blue) solid line indicates simulated delay differences over temperature for a magnetic field of 16 mT (100 mT).

The dispersion also caused the modulations on top of decays.[21] In the experimental signals these modulations occured blurred. The reason was thermal fluctuations which were induced by the coil around the vapor cell. The current through the windings produced additional heat which affected the vapor temperature when the maximum current of ±1 A was applied. On the other hand, the overall acquired delay was almost insensitive to these temperature fluctuations. Nevertheless, the simulations fit the data very well (as described in the theory section above). Furthermore, they reproduced the observed modulations. These modulations can be explained due to the frequency jitter of the emitted photons (i.e., spectral diffusion) which propagate through the medium.[21] The elongation of the wave packets was also directly connected to the presence of a rather broad spectrum (as described in [21]). In case of a narrow emission, the decay would be less distorted meaning that a fine-tuning at the scale of the QD's lifetime could lead to an entire separation of the polarization components.

Furthermore, the theoretical analysis allowed to investigate magnetic fields which exceed our experimental limitations. The results are shown in **Figure 5**a for the vapor temperature $T = 130$ °C which is equivalent to the one in the experiment. For zero magnetic field, all photons had the same arrival time at the single photon detectors. For increasing magnetic field the plot shows the increasing separation of arrival times. The working point of the experiment is marked. As already observed in the experimental results in Figure 4, the wavepackets still overlapped there. On the contrary, with a larger magnetic field up to 100 mT it would be possible to separate even this currently elongated photon wavepackets. This realistic magnetic field strength will be feasible in future experiments.

Finally, similar measurements were performed as in Figure 4, for different vapor temperatures. To better compare with the simulations in Figure 5a, the delay difference between σ^+- and σ^--components was plotted directly in Figure 5b. The data agreed very well with the simulated curve at 16 mT (solid blue line). As predicted, larger delay differences for every vapor temperature were expected for a magnetic field of 100 mT (solid light-blue line). This confirmed the role of temperature and magnetic field as tuning knobs for the delay.

4. Conclusion and Outlook

In conclusion, we have shown the extended control of the single photon propagation by an atomic vapor under the application of a magnetic field. In this study, two tuning knobs were used to control the photonic delay: vapor temperature and magnetic field. The latter becomes very interesting in order to achieve a

fine-tuning of the single photon delay. Indeed, applying a magnetic field can be done much faster than controlling the vapor temperature. Additionally, the combined use of vapor dispersion and magnetic field also results in an active routing of light, according to its polarization. Rather than previous studies, conducted with classical light, here we show that also single-photons can be routed via their interaction with an atomic medium. While current results only allowed a time separation between σ^+ and σ^- components of the order of the emitter's decay time, the theory predicts that much larger separation is achievable for higher magnetic field intensities. For the same reason, while current experimental setup allows for a slow change of the magnetic field orientation, faster equipments would allow the use of the described experiment for a fast photon multiplexing.

The shown results of the polarization and frequency selective photon routing is closely related to laser frequency locking. The introduced technique with the detection of two different circular polarization components of the quantum dot's emission is closely related to the "dichroic atomic vapor laser lock" (DAVLL). This allows, for example, for stabilizing a single quantum dot to an atomic transition. This is further discussed in ref. [29]. There, the particular delay would not be required, but rather the difference of the spectra of the two circular polarization components. Pinning the emission frequency to a universal reference is an important feature in the implementation of quantum networks, where multiple distinct sources need to be used (and matched in frequency).[34]

Acknowledgements

The authors acknowledge the work of H. Kammerlander from the Max Planck Institute's glass workshop who produced the cesium vapor cell. Further the work of W. Braun is acknowledged who produced the solenoids and the temperature controller for the cells. The authors acknowledge funding from the Deutsche Forschungsgemeinschaft in the project GE2737/5-1 and MI300/30-1. S.L.P. acknowledges the support of the Baden-Württemberg Stiftung Post-doc Eliteprogramm via the project "Hybride Quantensysteme für Quantensensorik". The research of IQST was supported financially by the Ministry of Science, Research and Arts Baden-Württemberg.

Conflict of Interest

The authors declare no conflict of interest.

Keywords

hot atomic vapor, hybrid quantum systems, quantum dots

Received: May 29, 2019
Revised: September 20, 2019
Published online: October 31, 2019

[1] P. D. Townsend, J. G. Rarity, P. R. Tapster, *Electron. Lett.* **1993**, *29*, 634.
[2] H. J. Kimble, M. Dagenais, L. Mandel, *Phys. Rev. Lett.* **1977**, *39*, 691.
[3] Th. Basché, W. E. Moerner, M. Orrit, H. Talon, *Phys. Rev. Lett.* **1992**, *69*, 1516.
[4] A. Gruber, A. Dräbenstedt, C. Tietz, L. Fleury, J. Wrachtrup, C. von Borczyskowski, *Science* **1997**, *276*, 2012.
[5] P. Michler, A. Kiraz, C. Becher, W. V. Schoenfeld, P. M. Petroff, Lidong Zhang, E. Hu, A. Imamoglu, *Science* **2000**, *290*, 2282.
[6] N. Akopian, N. H. Lindner, E. Poem, Y. Berlatzky, J. Avron, D. Gershoni, B. D. Gerardot, P. M. Petroff, *Phys. Rev. Lett.* **2006**, *96*, 130501.
[7] R. J. Young, R. M. Stevenson, P. Atkinson, K. Cooper, D. A. Ritchie, A. J. Shields, *New J. Phys.* **2006**, *8*, 29.
[8] S. Unsleber, C. Schneider, S. Maier, Yu-Ming He, S. Gerhardt, Chao-Yang Lu, J.-W. Pan, M. Kamp, S. Höfling, *Opt. Express* **2015**, *23*, 32977.
[9] N. Somaschi, V. Giesz, L. De Santis, J. C. Loredo, M. P. Almeida, G. Hornecker, S. L. Portalupi, T. Grange, C. Antón, J. Demory, C. Gómez, I. Sagnes, N. D. Lanzillotti-Kimura, A. Lemaítre, A. Auffeves, A. G. White, L. Lanco, P. Senellart, *Nat. Photonics* **2016**, *10*, 340.
[10] Xing Ding, Yu He, Z.-C. Duan, N. Gregersen, M.-C. Chen, S. Unsleber, S. Maier, C. Schneider, M. Kamp, S. Höfling, Chao-Yang Lu, J.-W. Pan, *Phys. Rev. Lett.* **2016**, *116*, 020401.
[11] P. Michler (Ed), *Quantum Dots for Quantum Information Technologies*, Springer International Publishing, Cham, Switzerland **2017**.
[12] D. F. Phillips, A. Fleischhauer, A. Mair, R. L. Walsworth, M. D. Lukin, *Phys. Rev. Lett.* **2001**, *86*, 783.
[13] J. A. Carruthers, T. Bieber, *J. Appl. Phys.* **1969**, *40*, 426.
[14] D. Grischkowsky, *Phys. Rev. A* **1973**, *7*, 2096.
[15] P. Siddons, Nia C. Bell, Yifei Cai, C. S. Adams, I. G. Hughes, *Nat. Photonics* **2009**, *3*, 225.
[16] P. Siddons, C. S. Adams, Ifan G. Hughes, *Phys. Rev. A* **2010**, *81*, 043838.
[17] N. Akopian, L. Wang, A. Rastelli, O. G. Schmidt, V. Zwiller, *Nat. Photonics* **2011**, *5*, 230.
[18] P. Siyushev, G. Stein, Jörg Wrachtrup, I. Gerhardt, *Nature* **2014**, *509*, 66.
[19] J. S. Wildmann, R. Trotta, J. Martín-Sánchez, E. Zallo, M. O'Steen, O. G. Schmidt, A. Rastelli, *Phys. Rev. B* **2015**, *92*, 235306.
[20] W. Kiefer, M. Rezai, J. Wrachtrup, I. Gerhardt, *Appl. Phys. B* **2016**, *122*, 38.
[21] H. Vural, S. L. Portalupi, J. Maisch, S. Kern, J. H. Weber, M. Jetter, J. Wrachtrup, R. Löw, I. Gerhardt, P. Michler, *Optica* **2018**, *5*, 367.
[22] F. Kaneda, P. G. Kwiat, High-Efficiency Single-Photon Generation via Large-Scale Active Time Multiplexing. *Arxiv* **2018**.
[23] S. Chu, S. Wong, *Phys. Rev. Lett.* **1982**, *48*, 738.
[24] T. Kroh, J. Wolters, A. Ahlrichs, A. W. Schell, A. Thoma, S. Reitzenstein, J. S. Wildmann, E. Zallo, R. Trotta, A. Rastelli, O. G. Schmidt, O. Benson, *Sci. Rep.* **2019**, *9*, 13728. https://www.nature.com/articles/s41598-019-50062-x.
[25] I. Gerhardt, *Opt. Lett.* **2018**, *43*, 5295.
[26] L. Weller, K. S. Kleinbach, M. A. Zentile, S. Knappe, I. G. Hughes, C. S. Adams, *Opt. Lett.* **2012**, *37*, 3405.
[27] B. Chéron, H. Gilles, J. Hamel, O. Moreau, H. Sorel, *J. Phys. III* **1994**, *4*, 401.
[28] K. L. Corwin, Z.-T. Lu, C. F. Hand, R. J. Epstein, C. E. Wieman, *Appl. Opt.* **1998**, *37*, 3295.
[29] M. Widmann, S. L. Portalupi, P. Michler, J. Wrachtrup, I. Gerhardt, *IEEE Photonics Technol. Lett.* **2018**, *30*, https://doi.org/10.1109/LPT.2018.2871770.
[30] R. N. Shakhmuratov, J. Odeurs, *Phys. Rev. A* **2008**, *77*, 033854.
[31] R. M. Camacho, M. V. Pack, J. C. Howell, *Phys. Rev. A* **2006**, *73*, 063812.
[32] S. L. Portalupi, M. Widmann, C. Nawrath, M. Jetter, P. Michler, J. Wrachtrup, I. Gerhardt, *Nat. Commun.* **2016**, *7*, 13632.
[33] M. A. Zentile, J. Keaveney, L. Weller, D. J. Whiting, C. S. Adams, I. G. Hughes, *Comput. Phys. Commun.* **2015**, *189*, 162.
[34] J. H. Weber, B. Kambs, J. Kettler, S. Kern, J. Maisch, H. Vural, M. Jetter, S. L. Portalupi, C. Becher, P. Michler, *Nat. Nanotechnol.* **2019**, *14*, 23.